The polarized spectral energy distribution of NGC 4151

F Marin, J Le cam, E Lopez-Rodriguez, M Kolehmainen, B Babler, M Meade

Monthly Notices
of the
ROYAL ASTRONOMICAL SOCIETY

MNRAS **496,** 215–222 (2020)
Advance Access publication 2020 June 3

doi:10.1093/mnras/staa1533

The polarized spectral energy distribution of NGC 4151

F. Marin [1]★ J. Le Cam,[2] E. Lopez-Rodriguez,[3] M. Kolehmainen,[1] B. L. Babler[4] and M. R. Meade[4]

[1] *Université de Strasbourg, CNRS, Observatoire Astronomique de Strasbourg, UMR 7550, F-67000 Strasbourg, France*
[2] *Institut d'optique Graduate School, 91120 Palaiseau, France*
[3] *SOFIA Science Center, NASA Ames Research Center, Moffett Field, CA 94035, USA*
[4] *Department of Astronomy, University of Wisconsin-Madison, Madison, WI 53706, USA*

Accepted 2020 May 25. Received 2020 May 15; in original form 2020 March 17

ABSTRACT

NGC 4151 is among the most well-studied Seyfert galaxies that does not suffer from strong obscuration along the observer's line of sight. This allows to probe the central active galactic nucleus (AGN) engine with photometry, spectroscopy, reverberation mapping, or interferometry. Yet, the broad-band polarization from NGC 4151 has been poorly examined in the past despite the fact that polarimetry gives us a much cleaner view of the AGN physics than photometry or spectroscopy alone. In this paper, we compile the 0.15–89.0 μm total and polarized fluxes of NGC 4151 from archival and new data in order to examine the physical processes at work in the heart of this AGN. We demonstrate that, from the optical to the near-infrared (IR) band, the polarized spectrum of NGC 4151 shows a much bluer power-law spectral index than that of the total flux, corroborating the presence of an optically thick, locally heated accretion flow, at least in its near-IR emitting radii. Specific signatures from the atmosphere of the accretion structure are tentatively found at the shortest ultraviolet (UV) wavelengths, before the onset of absorption opacity. Otherwise, dust scattering appears to be the dominant contributor from the near-UV to near-IR polarized spectrum, superimposed on to a weaker electron component. We also identify a change in the polarization processes from the near-IR to the mid-IR, most likely associated with the transition from Mie scattering to dichroic absorption from aligned dust grains in the dusty torus or narrow-line region. Finally, we present and discuss the very first far-infrared polarization measurement of NGC 4151 at 89 μm.

Key words: polarization – scattering – galaxies: active – galaxies: individual: NGC 4151 – galaxies: nuclei – galaxies: Seyfert.

1 INTRODUCTION

NGC 4151 holds a particular place in the field of active galactic nuclei (AGN). It was among the original list of the six '*extragalactic nebulae with high-excitation nuclear emission lines superposed on a normal G-type spectrum*' observed by Carl K. Seyfert, which later gave his name to a specific class of AGNs (Seyfert 1943). NGC 4151 is also one of the nearest galaxies to the Earth, $z \sim 0.00332$, which corresponds to a Hubble distance of 18.31 ± 1.31 Mpc (de Vaucouleurs et al. 1991). Its optical and ultraviolet (UV) fluxes are known to vary quite dramatically, resulting in a fluctuating optical-type classification. NGC 4151 changes from a Seyfert-1.5 type in the maximum activity state to a Seyfert-1.8 in the minimum state (Antonucci & Cohen 1983; Shapovalova et al. 2008). Indeed, long-term temporal behaviours of this AGN showed flux variation from a factor 2 to 6 over a period of 12 yr (Ulrich et al. 1991; Shapovalova et al. 2008). The X-ray flux of NGC 4151 is also known to be variable but is also very bright, explaining why it was one of the first Seyfert galaxies to be detected in the high-energy sky by the Uhuru Satellite (Gursky et al. 1971; Warwick, Done & Smith 1995). A complete 0.1–100 keV coverage of the source showed that the X-ray spectrum of NGC 4151 is a complex association of emitting and absorbing components arising from various locations, from the central engine to the extended polar outflows of the AGN (e.g. Schurch & Warwick 2002; Schurch et al. 2004). This complexity underlies a fundamental question: are all AGNs such convoluted systems or is NGC 4151 unique? In order to better understand the intrinsic physics and structure of Seyfert galaxies, it becomes of great interest to determine whether this Seyfert galaxy is an archetype of its class or very far from it (Zdziarski et al. 2002).

The proximity of NGC 4151 allowed to measure several of its prime attributes. The narrow-line region (NLR) of this AGN has an inclination close to 45° (Fischer et al. 2013, 2014; Marin 2016)

★ E-mail: frederic.marin@astro.unistra.fr

with the north side out of the plane of sky away from our line-of-sight (LOS), which makes NGC 4151 an intermediate-type Seyfert galaxy. This means that we are able to directly see the central engine (a supermassive black hole and its associated putative accretion disc) through the dust funnel of the circumnuclear gas and dust distribution that characterizes AGNs (see the fundamental paper on the subject by Antonucci 1993). This dusty equatorial obscurer is the reason why we cannot see the central engine in type-2 AGNs where the observer's LOS intercepts this optically thick medium. The possibility to peer the central engine in NGC 4151 allowed to estimate its black hole mass to be of the order of 4×10^7 $M_\odot$ (Bentz et al. 2006; Onken et al. 2007). The supermassive black hole appears to be maximally spinning (Cackett et al. 2014) and its inferred mass accretion rate is about 0.013 $M_\odot$ yr^{-1} (Crenshaw & Kraemer 2007). The putative geometrically thin, optically thick, accretion disc that surrounds the black hole is responsible for the multitemperature thermal emission that produces a UV-to-optical signature called the Big Blue Bump. At the end of the accretion disc lies the broad emission line region (BELR) that is responsible for the detected broad emission lines in the UV, optical, and near-infrared (near-IR) spectrum of AGNs (Gaskell 2009). The size of the BELR is object dependent, but it is generally admitted that it lies between the accretion disc and the inner radius of the dusty circumnuclear region. In NGC 4151, the radius at which dust grains start to survive the intense radiation field was measured because of reverberation mapping studies and is of the order of 0.04 pc (Minezaki et al. 2004). Dust is responsible for another detectable feature in the spectral energy distribution (SED) of AGN, usually referred to as the IR bump and most likely associated with re-radiated emission from the dust grains.

The superposition of the emission lines and the IR re-emission on to the UV/optical continuum makes it difficult to precisely measure the shape and the peak of the Big Blue Bump. This is unfortunate since the Big Blue Bump provides critical information on the structure and condition of the innermost AGN components. In order to isolate the true SED of the central component, it is advised to look at the polarized light of the AGN. Indeed, the polarized flux shaves off the unpolarized line emission from the extended AGN polar outflows or the host galaxy (Kishimoto et al. 2004, 2008). In addition, polarimetry can detect variations in the emission/scattering physics because of two additional and independent parameters: the polarization degree and polarization position angle (Kishimoto et al. 2008; Marin 2018). In this paper, we thus investigate the polarized light of NGC 4151 because of archival polarimetric campaigns and compile, for the first time, its UV-to-IR polarized SED. We aim at characterizing the emission from the Big Blue Bump, i.e. from the accretion disc itself, by eliminating the parasitic light from the BELR and from the dusty components in the near-IR. Additionally, we want to determine what are the dominant mechanisms that are responsible for the observed polarization from the UV to the far-IR band, allowing us to build a better picture of the central AGN components. The paper is organized as follows: Section 2 describes the archive data and examines the total and polarized SED, which are further discussed in Section 3. In Section 4, we present the conclusions.

2 THE POLARIZED FLUX SPECTRUM OF NGC 4151

2.1 Compiling the data

We skimmed through the SAO/NASA Astrophysics Data System digital library and gathered all the publications reporting polarization measurements in NGC 4151. We found 19 papers spanning from 1971 to 2018. Two papers reported circular polarization measurements (Nikulin, Kuvshinov & Severny 1971; Angel et al. 1976) and, since we are interested in linear polarization only (the thermally emitted Big Blue Bump should not produce intrinsically circularly polarized light), we safely discarded them.[1] Due to the diversity of instruments, the polarimetric data are also spanning from apertures that widely vary from sub-arcsecond scales to more than 40 arcsec. It is obvious that we cannot reconstruct a polarized SED using dramatically different apertures so we focused on apertures lower than 10 arcsec. At an heliocentric distance of 18.31 Mpc, this corresponds to a linear size of 0.88 kpc. Since AGN polar outflows are often optically detected up to a projected distance of 1 kpc (see, e.g. Schmitt & Kinney 1996), we ensure that the polarized SED mostly accounts for the AGN flux, not the host galaxy. Finally, we favoured publications with spectropolarimetric data instead of measurements taken with broad filters. This allows us to have a much more precise reconstruction of the shape of the Big Blue Bump. We ended up with seven publications covering as many wavelengths as possible from the optical to the near/mid-IR (see Table 1). To account for the *UV* band, we retrieved the old and unpublished polarization measurements taken by the Wisconsin Ultraviolet Photo Polarimeter Experiment (WUPPE; Code et al. 1993; Nordsieck et al. 1994). Five polarimetric observations in the 0.15–0.32 μm band were obtained with WUPPE and compiled by the WUPPE team into a 3136 s long exposure spectrum visible in Fig. 1. The observations were temporally close enough that variability was not an issue for stacking the Stokes parameters. We have also included newly acquired imaging polarimetric data at 89 μm using the High-resolution Airborne Wideband Camera/Polarimeter (HAWC+) onboard the 2.7-m NASA's Stratospheric Observatory for Infrared Astronomy (SOFIA). These observations are part of an AGN polarimetric survey at far-IR wavelengths under the program 07\0032 (PI: Lopez-Rodriguez). Observations were performed on January the 28th, 2020, with a total on-source time of 3360 s and will be presented in detail in a follow-up manuscript (Lopez-Rodriguez et al. in prep.). For the goal of this project, we performed aperture photometry within the beam size of 7.″80 (0.69 kpc) at 89 μm and estimated that the nucleus of NGC 4151 is unpolarized (0.9 ± 0.8 per cent) with an undetermined position angle of polarization. The final compilation of published, archival, and new polarimetric measurements of NGC 4151 is presented in Table 1. The total and polarized fluxes will be presented in Fig. 2, while the polarization degrees and position angles will be shown in Fig. 4.

2.2 Examination of the total and polarized fluxes

We present in Fig. 2 the broad-band, 0.15–89.0 μm, total flux (top), and polarized flux (bottom) spectra of NGC 4151. The total flux is entirely coherent with past measurements (Kriss et al. 1995; Alexander et al. 1999) and with the nuclear SED retrieved from the NASA/IPAC Extragalactic Database. The nuclear SED, shown in the shaded grey in Fig. 2, is the averaged SED compiled from continuum flux measurements with apertures lower than 10 arcsec. The thickness of the grey area corresponds to the observed flux fluctuations (including the error bars) and the missing data were linearly interpolated between two contiguous points. We note that

[1] The optical circular polarization measurement of Nikulin et al. (1971) has been contradicted by Gehrels (1972).

Table 1. Catalogue of published, archival (WUPPE), and new (SOFIA) polarimetric measurements of NGC 4151. The first column is the reference paper, the second column is the instrument used for the measurement, the third column is the waveband or filters used during the observation and the fourth column is the observation aperture (in arcseconds). The exact instrument aperture is not know in the case of Axon et al. (1994)'s publication but it is likely to be of the order of 4 arcsec, see the optical spectropolarimetry of 3C 234 taken with the same instrument by Young et al. (1998).

Reference	Instrument	Waveband (μm)	Aperture (arcsec)
MAST archives	Wisconsin Ultraviolet Photo Polarimeter Experiment (WUPPE)	0.15–0.32	4.2 arcsec
Thompson et al. (1979)	Steward Observatory 2.25 m telescope using the UCSD 200-channel Digicon	0.32–0.36	2.25 arcsec
Schmidt & Miller (1980)	Lick Observatory (3m Shane telescope)	0.37–0.71	2.8 arcsec
Axon et al. (1994)	4.5m William Herschel Telescope	0.48–0.75	?
Kruszewski (1977)	Steward 229 cm, Catalina 154 cm, Mt. Lemmon 102 cm reflectors	R (0.86), V (0.55), G (0.52), B (0.44), U (0.36),N (0.33)	10 arcsec
Ruiz et al. (2003)	Dual-beam polarimeter IRPOL2 at the United Kingdom Infrared Telescope (UKIRT)	J(1.23), H(1.64)	1 arcsec
Kemp et al. (1977)	Steward 2.25 m telescope	2.22	7.8 arcsec
Lopez-Rodriguez et al. (2018)	CanariCam on the 10.4-m Gran Telescopio CANARIAS	8–13	0.4 arcsec
Lopez-Rodriguez et al. (in preparation)	HAWC+ onboard the 2.7-m Stratospheric Observatory for Infrared Astronomy (SOFIA)	89	7.8 arcsec

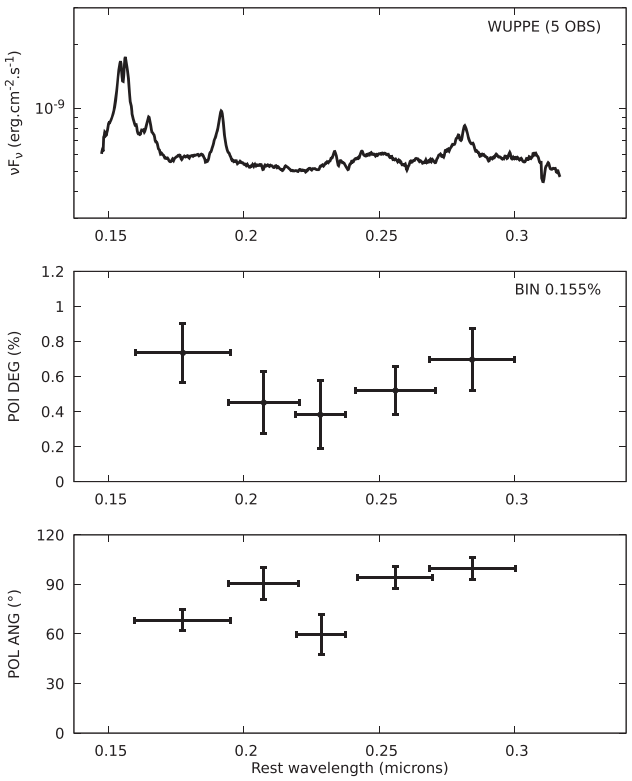

Figure 1. Unpublished MAST archival compilation of all the polarimetric observations of NGC 4151 made with WUPPE. It sums up five observation campaigns taken between 1995 March 4 and 13 for a total of 3136 s.

due to the variable nature of NGC 4151 in the UV and optical bands, and since it is a composite spectrum aggregating about 40 yr of measurements, it is not gainful to fit the total flux data points in order to obtain a representative spectral index for the underlying continuum. Although the intensity spectrum is coherent with the nuclear data averaged from NED, it has been shown that the continuum can vary by a factor of 6 in less than 10 yr, impeding a trustworthy estimation of the spectral index from the optical to near-IR waveband (≈0.5–1 μm). We illustrate this in Fig. 3, where we can see that the spectral index of the UV and optical/near-IR power laws underlying the continuum are drastically different due to variability. Fortunately, in the near-to-mid IR, where the accretion disc spectrum starts to be hidden under the hot dust thermal emission from the equatorial dusty region, variability is less of an issue (see Fig. 3). This allowed us to fit the IR (1–12 μm) spectral index from the total flux SED: $F_\nu \propto \nu^{-1.33}$. This spectral index is entirely consistent with the average value of -1.48 ± 0.30 reported by Alonso-Herrero et al. (2003) for the IR (1–16 μm) spectral index of a sample of 22 Seyfert 1–1.5 galaxies.

To unveil the signature of the external parts of the putative accretion disc that should produce a much bluer spectral index than the total flux from the optical to the near-IR, we plot the polarized flux of NGC 4151 in Fig. 2 (bottom spectrum). The data are entirely consistent with partially to-unpolarized line emissions superposed on a smooth polarized continuum (Schmidt & Miller 1980). The optical-to-near-IR spectral slope is clearly more pronounced (bluer) in polarized flux and extends up to 2.2 μm. Yet again, the non-simultaneity of the optical and near-IR observations makes it unproductive to measure a spectral index. However, it has been demonstrated by Gaskell et al. (2012) that the polarized flux of NGC 4151 follows the total flux with a lag of a few days, allowing us to correlate the two quantities in order to suppress the variable component. This permits us to provide a qualitative measurement of the difference between the spectral index of the total and polarized fluxes. From power least-squares fittings, we find a difference of ∼0.6. This is entirely consistent with Kishimoto et al. (2008), in which a optical-to-near-IR power-law spectral index difference of ∼0.74 between the total and polarized fluxes of their quasar sample can be estimated from their fig. 1. Although we cannot precisely measure the optical-to-near-IR spectral slope in NGC 4151 using a multi-epoch composite spectrum, we confirm the methodology of Kishimoto et al. (2008): the polarized light spectrum of NGC 4151 seems to corroborate the existence of an optically thick, thermally heated accretion disc structure, at least in its outer near-IR emitting radii. Single epoch, multiwavelength polarimetric data are required to get a quantitative conclusion.

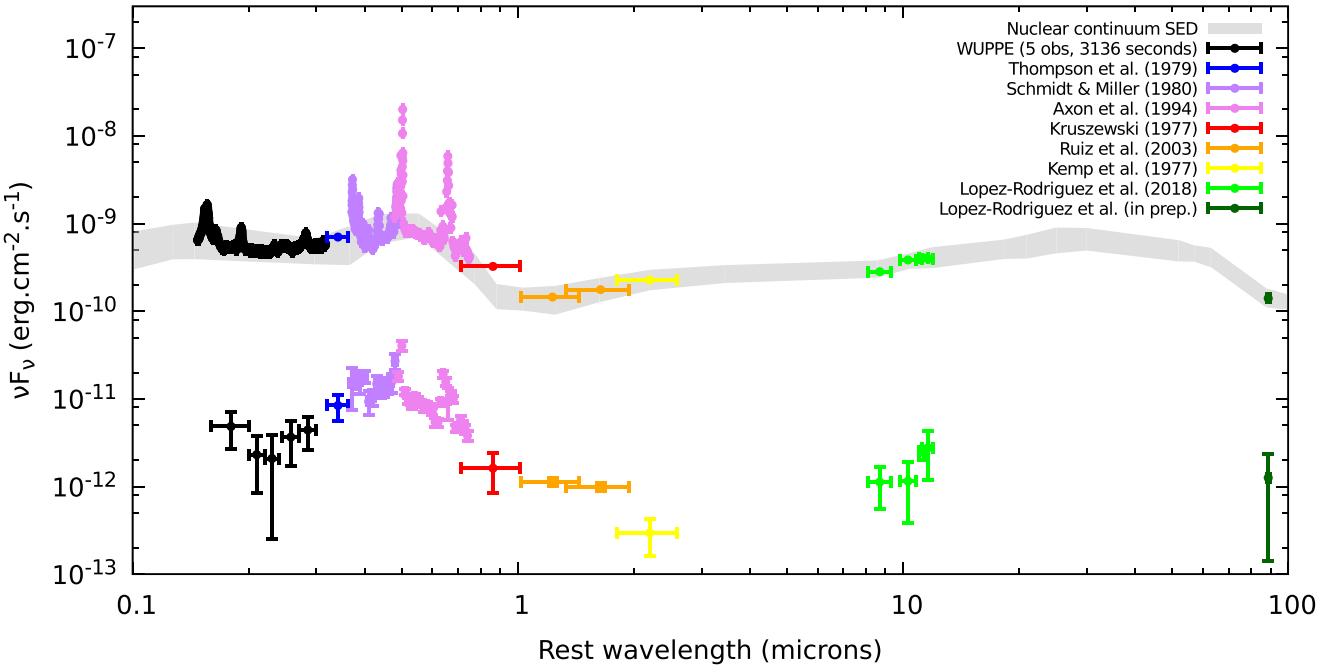

Figure 2. Broad-band 0.15–89.0 μm total flux (top) and polarized flux (bottom) spectra of NGC 4151 measured from various instruments (see Table 1). The grey region represents the averaged nuclear continuum SED extracted from the NASA/IPAC Extragalactic Database.

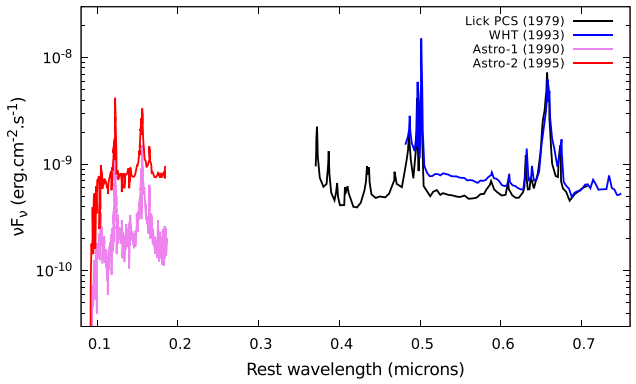

Figure 3. Example of the strong UV and optical variability in NGC 4151. The far-UV fluxes are from the Hopkins Ultraviolet Telescope on Astro-1 (Kriss et al. 1992) and Astro-2 (Kriss et al. 1995), while the optical fluxes are from the Pockels cell spectropolarimeter of Lick Observatory (Schmidt & Miller 1980) and the 4.5 m William Herschel Telescope by Axon et al. (1994).

2.2.1 Polarization degree and angle

Looking at the polarization degree of NGC 4151 in Fig. 4, we observe a rather wavelength-dependent spectrum. We first made sure that the polarization degree and angle continua were not subject to variability due to the different epochs of observation. Gaskell et al. (2012) demonstrated that the *B*-band degree and angle of polarization of NGC 4151 did not vary (were constant within the observational error bars) between 1997 and 2003. A similar conclusion can be drawn between 0.48 and 0.71 μm, where the polarized observations of Schmidt & Miller (1980) and Axon et al. (1994) indicate that the degree and angle of polarization remained constant over ∼15 yr. We are thus sure that intrinsic variability, such as synchrotron polarization induced in a failed jet, is not an issue here. The polarization we report has been corrected for instrumental polarization by the respective authors and interstellar polarization is not an issue. NGC 4151 is situated close to the North Galactic Pole (RA: 182°.635745, Dec.: 39°.405730), so the interstellar contribution is negligible. It was measured to be 0.07 per cent close to 0.44 μm by Kruszewski (1977). The only remaining source of extra-nuclear light is the host galaxy, a (R')SAB(rs)ab galaxy type according to de Vaucouleurs et al. (1991). The starlight of such spiral galaxy usually peaks in the 0.7–2 μm band (in νF_ν, Polletta et al. 2007) and, in the case of NGC 4151, the AGN light should dominate shortwards of 0.5 μm (Schmidt & Miller 1980). So, where does the strong wavelength dependence of the UV polarization come from? If electron scattering was the sole physical mechanism responsible for the observed polarization, both the polarization degree and angle would have been constant from the UV to the near-IR. Here, the increase of the polarization degree shortwards 0.23 μm is qualitatively explained by the accretion disc atmosphere models presented by Blaes & Agol (1996). In order to explain and reproduce far-UV polarimetric observations of AGNs, the authors developed a numerical tool to calculate fully self-consistent models of pure-hydrogen disc atmospheres. They included the effects of opacity absorption (both from free–free absorption and photoionization) and found that UV polarization from disc atmospheres rises at shorter wavelengths. A maximum is reached between 0.1 and 0.2 μm, where a rotation on the polarization position angle might occur, depending on the effective temperature and surface gravity of the model (see figs 2 and 3 in Blaes & Agol 1996). Below the Lyman edge (0.0912 μm) the polarization is expected to drop dramatically before rising up to several per cents in the extreme-UV. Unfortunately, there is no polarimetric data on NGC 4151 below 0.16 μm so a far-UV spectropolarimeter is needed to confirm that the rise of polarization we see at 0.16–0.2 μm in Fig. 4 is real.

From 0.2 to 0.5 μm the polarization degree rises, from ∼0.5 per cent to ∼2.0 per cent. This wavelength dependence is the

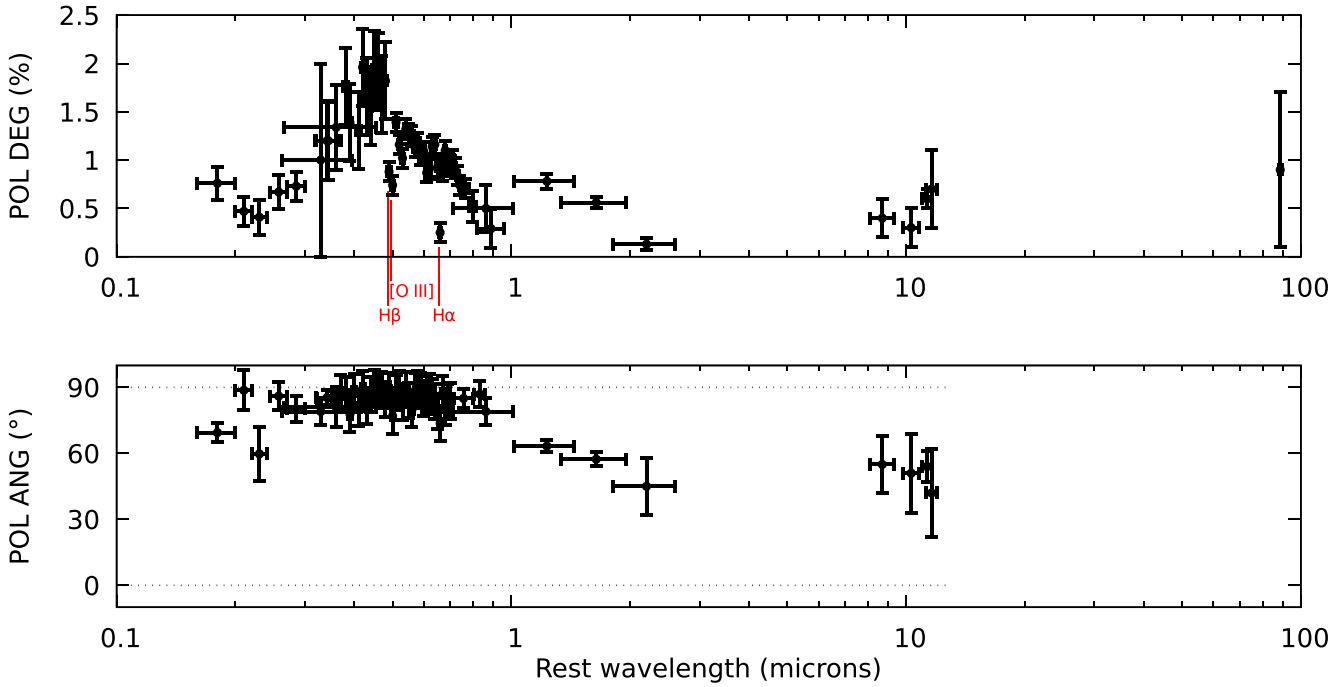

Figure 4. Broad-band polarization degree (top) and polarization angle (bottom) of NGC 4151. The polarization angle was reduced to the interval 0–90° (see references in Table 1). The polarization angle at 89 μm is undefined because the core is consistent with an unpolarized source.

signature of dust scattering, most likely from the inner surfaces of the dusty circumnuclear region and, less likely, from the dust grains inside the polar regions. The polarization position angle is close to 90° which, when compared to the 450 milliarsec radio structure along a position angle ≈83° observed with VLBI/Merlin (Harrison et al. 1986), indicates that equatorial scattering dominates. Indeed, subtracting the radio position angle from the measured polarization angle gives a result close to 0°. This means that the polarization position angle is parallel to the small-scale radio axis, hence scattering mainly occurs along the equatorial plane and not inside the polar outflows. It was shown by Goosmann & Gaskell (2007) that an isolated dusty torus, viewed at an inclination close to its half-opening angle is able to produce a polarization degree that rises at longer wavelengths, up to several per cents. A more complex structure inclined at 45°, including an accretion disc, a BELR, a circumnuclear obscurer, and ionized polar winds is also capable of producing a polarization degree that increases with increasing wavelengths, together with a parallel polarization position angle (Marin et al. 2012). Mie scattering is thus the dominant mechanism producing the 1–10 arcsec near-UV/optical polarization in NGC 4151. Electron scattering also occurs but is less dominant, otherwise the polarization degree would be grayer, such as seen in the first arcsecond around the core of NGC 1068 (Miller, Goodrich & Mathews 1991; Antonucci, Hurt & Miller 1994; Marin 2018). Interestingly, our result differs from the conclusions of Kishimoto et al. (2008) who found that electron scattering is the dominant scattering mechanism in their sample. This difference is actually due to target selection: NGC 4151 is a low-luminosity AGN (Seyfert galaxy), while Kishimoto et al. (2008)'s sample consists of six high-luminosity AGNs (quasars). Because quasars are much brighter than Seyferts, radiative pressure tends to destroy a larger fraction of dust in the close environment of the AGN, resulting in circumnuclear dusty regions that are much thinner (geometrically flattened along the equatorial plane) than in the Seyfert's case (Lawrence & Elvis 1982; Sazonov, Churazov & Krivonos 2015; Marin 2016). In particular, Sazonov et al. (2015) found that low-luminosity AGNs tend to have more massive torus, situated closer to the central engine, than quasars. This results in a larger solid angle for light-dust interaction at the inner radius of the circumnuclear dust in NGC 4151 than for quasars, hence a stronger impact of Mie scattering on to the observed polarization. Our results conveniently confirm that low-luminosity AGNs are likely to be embedded in a dustier environment than quasars.

From 0.5 to 1.0 μm, the polarization degree decreases due to the onset of the flux dominance from the host galaxy (Schmidt & Miller 1980). The dilution is due to unpolarized starlight that peaks in this regime. The same behaviour was observed in the polarized spectrum of NGC 1068 (Marin 2018). The polarization angle remains constant, indicating that equatorial scattering still dominates from 0.5 to 1.0 μm. The polarization position angle only deviates from the parallel alignment after 1.0 μm. The polarization angle rotates from ∼83° to 45° at 2.2 μm then stabilizes up to the mid-IR (8–12 μm). This variation is of particular interest because it clearly tells us that the physical mechanisms responsible for the production of polarization in the IR band in NGC 4151 is no longer dust scattering, as in the optical. Such finding must be put in the light of an infrared study of the polarization in NGC 4151 by Lopez-Rodriguez et al. (2018). In their work, the authors stated 'The nearly constant degree and [angle] of polarization from 1 to 12 μm strongly suggest that a single polarization mechanism dominates in the core of NGC 4151'. We entirely agree with them. However, they also stated that 'scattering off optically thick dust ... is consistent with the observed nearly constant degree and [polarization angle]'. This is a reasonable assumption only if the 1–12 μm band is isolated from the optical and UV polarization data. In our extended study, we showed that dust scattering occurs in the optical but is no longer the main

mechanism producing polarization in the infrared due to the rotation of the polarization angle.[2] Another supporting clue for this statement is the fact that the bump in polarization around 1–2 μm cannot be produced by Mie scattering alone (Young et al. 1995; Efstathiou, McCall & Hough 1997). In fact, looking at fig. 3 from Lopez-Rodriguez et al. (2018), dichroic absorption from aligned dust grains appears to be a better explanation for the wavelength-dependent IR polarization in NGC 4151. This is also supported by the simulations from Young et al. (1995), where a dichroic component is necessary to produce the expected polarization degrees longward of 1.5 μm (see their fig. 6, bottom panel). In-between 12 and 89 μm, another change in the polarization process happens, since polarization from magnetically aligned dust grains dominates over other polarization mechanisms (e.g. dust/electron scattering, dichroic absorption, and synchrotron emission). The null polarization at 89 μm can then arise from 1) a dominant turbulent magnetic field in the central tens parsecs from the core, and/or 2) a depolarization effect due to the large beam (7.80 arcsec, 0.68 kpc), averaging a more complex underlying field.

3 DISCUSSION

The polarimetric data from WUPPE must be taken with caution. In the UV regime, polarimetric measurements of AGN ionizing fluxes have a low signal-to-noise ratio. For this reason, unbinned polarization plots always appear to show greater polarization than binned results. This is due to the fact that polarization is a positive quantity. When calculating the average polarization over a wavelength range, the mean values of the Stokes parameters Q and U are error-weighted but WUPPE suffered from instrumental issues that could not be reliably calibrated. For this reason, there is no data between 2368 and 2430 Å, and the measurements in the 1600–3000 Å band should be analyzed with circumspection. The error bars in Fig. 1 are 1σ errors and the Q and U values are in different quadrants of the Q–U plane, which partially explains why the polarization angle may disagree so much between two consecutive bins (e.g. the 1600–2000 and the 2000–2200 Å bins). Finally, there is a correction to the polarimetric value that is not the simple error-weighted means of $\sqrt{\langle Q\rangle^2 + \langle U\rangle^2}$. The adjustment of the final polarimetric values as a function of polarimetric signal to noise is described in Nordsieck (1976).

It was shown by Impey et al. (1995) and Koratkar et al. (1995) that at least three high-redshift AGNs have a remarkably high polarization in the far-UV. One of the best examples is PG 1630+377 ($z \approx 1.48$). Its UV polarization degree rises rapidly up to 20 per cent below the Lyman edge, a value that is usually found in blazing sources. Numerous scenarios for explaining such polarization features has been proposed by Koratkar et al. (1995), including Faraday screens covering highly polarized continuum sources and geometric dilution. We now know that source obscuration is not an option as the inclination of NGC 4151 is such that we can directly see its central engine, allowing reverberation mapping studies (e.g. Bentz et al. 2006; Gaskell et al. 2012). Simulations by Blaes & Agol (1996) also failed to reproduce such dramatic value using a pure-hydrogen disc atmosphere model. More recently, new computations by Chang, Lee & Yang (2017) tried to compute the Rayleigh polarization emerging from scattered radiation around the Lyman alpha wavelength in thick neutral regions but they could not apply their results to PG 1630+377. One of the reasons for such slow progresses is the lack of data. We only have a handful of UV polarimetric measurements from high-redshift quasars ($z > 0.5$).

The 1–12 μm polarization of six Seyfert galaxies shows a diverse set of physical processes arising from its cores (Lopez-Rodriguez et al. 2018). For radio-quiet obscured AGN, the polarization is mainly arising from dichroic absorption by the dusty obscured surrounding the active nuclei or host galaxy. However, for NGC 4151, an un-obscured radio-quiet AGN, the physical component producing the IR polarization is difficult to identify. The reason is due to the competing polarization mechanisms of the several physical components within the beam size of the observations. We here provide a potential interpretation based on the shape of the 1–89 μm polarized spectrum and radiative alignment torque mechanism by Lee et al. (2019). These authors show that the polarization peak arising from dichroic absorption by aligned dust grains changes as a function of the radiation field, extinction, and dust grain properties. To reproduce our 1–2 μm bump polarization, a direct view to the source with low extinction, $A_v \leq 5$, oblate grains with axial ratio of 1.5, and dust grains expose to weak radiation field are required (fig. 7 in Lee et al. 2019). This physical environment predicts a negligible emissive polarization at 89 μm with a rise of polarization at longer wavelengths (fig. 10 in Lee et al. 2019). We interpret these results as that our 1–89 μm polarization arises from elongated and aligned dust absorption in the 1–12 μm wavelength range and emission at 89 μm. As the dust grains are exposed to weak radiation field, the dust may be located in the outer areas of the torus or NLR as suggested by Lopez-Rodriguez et al. (2018). Our approach has shown that a detailed analysis of the total and polarized flux, the degree, and position angle of polarization, together with high angular resolution observations, is a powerful tool to identify the most likely mechanisms producing polarization in the whole electromagnetic spectrum.

4 CONCLUSIONS

We have compiled, for the first time, the polarized SED of NGC 4151, one of the archetypal pole-on Seyfert galaxies. Despite the inherent problem of UV and optical variability, we have demonstrated that the optical-to-near-IR power-law spectral index of NGC 4151 is much bluer in polarized flux. This is in perfect agreement with past studies of quasars polarized SED, strengthening the case for the use of polarimetry to unveil the true nature of the Big Blue Bump. We have analyzed the wavelength-dependent polarization of this object and found a potential signature of the accretion disc atmosphere in the shortest wavelengths. However, due to the unreliability of the instrument in this waveband, new UV polarimetric observations are necessary. We have also established that the continuum polarization of NGC 4151 is mainly due to dust scattering from the near-UV to the near-IR. Compared to the sample of Kishimoto et al. (2008), who found that electron scattering dominates in higher luminosity AGNs, our result tend to confirm that low-luminosity objects such as NGC 4151 are embedded in dustier environments. A smooth rotation of the polarization position angle between 1 and 2.2 μm identified a change in the polarization mechanism that we attribute to the onset of dichroic absorption from aligned dust grains. In the far-IR, polarization from dichroic absorption becomes less dominant and polarized emission from elongated and aligned dust grains prevails. Our results demonstrate that single epoch, broad-band, polarimetric

[2]Lopez-Rodriguez et al. (2018) did not account for the infrared polarization measurement obtained by Kemp et al. (1977) at 2.2 μm that would have otherwise better highlighted the smooth variation of the polarization angle in the near-IR band in their study.

measurements are necessary to unveil the physical mechanisms that produce polarization in the heart of AGNs. We thus advocate for new polarimeters that could cover the a large fraction of the UV-to-IR electromagnetic spectrum.

In addition, WUPPE data are the only spectropolarimetric UV measurements of NGC 4151 so far. This pull the trigger on the importance of new UV spectropolarimeters in the future. If we aim at investigating the UV properties of nearby AGNs, it is necessary to probe the shortest wavelengths in order to uncover the potential signatures from the accretion disc or its atmosphere. Spectropolarimetric observations of nearby AGN at rest wavelengths below the Lyman edge are thus mandatory to push forward the analysis. Future spatial instruments such as POLLUX, a high-resolution UV spectropolarimeter proposed for the 15-meter primary mirror option of LUVOIR (Bouret et al. 2018; Marin et al. 2018), or satellites at higher energies such as IXPE (Weisskopf et al. 2016; Marin & Weisskopf 2017) are necessary to shed light on this topic. Furthermore, high-spatial resolution observations in the 1–200 μm can provide us with detailed information about the physical scales of the dusty structure obscuring the AGN as well as the presence/absence of magnetic fields in the accretion flow to the active nuclei. Future ground-based 30-m class telescopes and space-based telescopes equipped with sensitive polarimeters, such as SPICA (Adami et al. 2019) and Origins (Staguhn et al. 2018), are thus also mandatory.

ACKNOWLEDGEMENTS

We would like to thank the anonymous referee for taking the time to write an encouraging report on our paper. The authors are grateful to Robert 'Ski' Antonucci for his remarks and suggestions that improved the quality of this article. FM would like to thank the Centre national d'études spatiales (CNES) who funded his post-doctoral grant 'Probing the geometry and physics of active galactic nuclei with ultraviolet and X-ray polarized radiative transfer'. Based partially on observations made with the NASA/DLR SOFIA under the 07\0032 Program. SOFIA is jointly operated by the Universities Space Research Association, Inc., under NASA contract NAS2-97001, and the Deutsches SOFIA Institut (DSI) under DLR contract 50 OK 0901 to the University of Stuttgart.

REFERENCES

Adami O.-A., Rodriguez L., Poglitsch A., Bounissou S., Reveret V., Aliane A., Goudon V., Dussopt L., 2019, Appl. Opt., 58, 398
Alexander T., Sturm E., Lutz D., Sternberg A., Netzer H., Genzel R., 1999, ApJ, 512, 204
Alonso-Herrero A., Quillen A. C., Rieke G. H., Ivanov V. D., Efstathiou A., 2003, ApJ, 126, 81
Angel J. R. P., Stockman H. S., Woolf N. J., Beaver E. A., Martin P. G., 1976, ApJ, 206, L5
Antonucci R., 1993, ARA&A, 31, 473
Antonucci R. R. J., Cohen R. D., 1983, ApJ, 271, 564
Antonucci R., Hurt T., Miller J., 1994, ApJ, 430, 210
Axon D. J., Hough J. H., Young S., Inglis M., 1994, Ap&SS, 216, 379
Bentz M. C. et al., 2006, ApJ, 651, 775
Blaes O., Agol E., 1996, ApJ, 469, L41
Bouret J.-C. et al., 2018, in Proc. SPIE Conf. Ser. Vol. 10699, Space Telescopes and Instrumentation 2018: Ultraviolet to Gamma Ray. SPIE, Bellingham, p. 106993B
Cackett E. M., Zoghbi A., Reynolds C., Fabian A. C., Kara E., Uttley P., Wilkins D. R., 2014, MNRAS, 438, 2980
Chang S.-J., Lee H.-W., Yang Y., 2017, MNRAS, 464, 5018
Code A. D. et al., 1993, ApJ, 403, L63
Crenshaw D. M., Kraemer S. B., 2007, ApJ, 659, 250
de Vaucouleurs G., de Vaucouleurs A., Corwin H. G., Jr, Buta R. J., Paturel G., Fouqué P., 1991, Third Reference Catalogue of Bright Galaxies. Springer, Berlin
Efstathiou A., McCall A., Hough J. H., 1997, MNRAS, 285, 102
Fischer T. C., Crenshaw D. M., Kraemer S. B., Schmitt H. R., 2013, ApJ, 209, 1
Fischer T. C., Crenshaw D. M., Kraemer S. B., Schmitt H. R., Turner T. J., 2014, ApJ, 785, 25
Gaskell C. M., 2009, New Astron. Rev., 53, 140
Gaskell C. M., Goosmann R. W., Merkulova N. I., Shakhovskoy N. M., Shoji M., 2012, ApJ, 749, 148
Gehrels T., 1972, ApJ, 173, L23
Goosmann R. W., Gaskell C. M., 2007, A&A, 465, 129
Gursky H., Kellogg E. M., Leong C., Tananbaum H., Giacconi R., 1971, ApJ, 165, L43
Harrison B., Pedlar A., Unger S. W., Burgess P., Graham D. A., Preuss E., 1986, MNRAS, 218, 775
Impey C. D., Malkan M. A., Webb W., Petry C. E., 1995, ApJ, 440, 80
Kemp J. C., Rieke G. H., Lebofsky M. J., Coyne G. V., 1977, ApJ, 215, L107
Kishimoto M., Antonucci R., Boisson C., Blaes O., 2004, MNRAS, 354, 1065
Kishimoto M., Antonucci R., Blaes O., Lawrence A., Boisson C., Albrecht M., Leipski C., 2008, Nature, 454, 492
Koratkar A., Antonucci R. R. J., Goodrich R. W., Bushouse H., Kinney A. L., 1995, ApJ, 450, 501
Kriss G. A. et al., 1992, ApJ, 392, 485
Kriss G. A., Davidsen A. F., Zheng W., Kruk J. W., Espey B. R., 1995, ApJ, 454, L7
Kruszewski A., 1977, Acta Astron., 27, 319
Lawrence A., Elvis M., 1982, ApJ, 256, 410
Lee H., Hoang T., Le N., Cho J., 2019, preprint (arXiv:1911.00654)
Lopez-Rodriguez E. et al., 2018, MNRAS, 478, 2350
Marin F., 2016, MNRAS, 460, 3679
Marin F., 2018, MNRAS, 479, 3142
Marin F., Weisskopf M. C., 2017, in Reylé C., Di Matteo P., Herpin F., Lagadec E., Lançon A., Meliani Z., Royer F., eds, SF2A-2017: Proceedings of the Annual meeting of the French Society of Astronomy and Astrophysics. French Society of Astronomy & Astrophysics, Paris, p. 173
Marin F., Goosmann R. W., Gaskell C. M., Porquet D., Dovčiak M., 2012, A&A, 548, A121
Marin F. et al., 2018, in Matteo P. D., Billebaud F., Herpin F., Lagarde N., Marquette J.-B., Robin A., Venot O., eds, SF2A-2018: Proceedings of the Annual meeting of the French Society of Astronomy and Astrophysics. French Society of Astronomy & Astrophysics, Paris, p. 71
Miller J. S., Goodrich R. W., Mathews W. G., 1991, ApJ, 378, 47
Minezaki T., Yoshii Y., Kobayashi Y., Enya K., Suganuma M., Tomita H., Aoki T., Peterson B. A., 2004, ApJ, 600, L35
Nikulin N. S., Kuvshinov V. M., Severny A. B., 1971, ApJ, 170, L53
Nordsieck K. H., 1976, ApJ, 209, 653
Nordsieck K. H., Code A. D., Anderson C. M., Meade M. R., Babler B., Michalski D. E., Pfeifer R. H., Jones T. E., 1994, Exploring Ultraviolet Astronomical Polarimetry: Results from the Wisconsin Ultraviolet Photo-Polarimeter Experiment (WUPPE), SPIE, San Diego, p. 2
Onken C. A. et al., 2007, ApJ, 670, 105
Polletta M. et al., 2007, ApJ, 663, 81
Ruiz M., Young S., Packham C., Alexander D. M., Hough J. H., 2003, MNRAS, 340, 733
Sazonov S., Churazov E., Krivonos R., 2015, MNRAS, 454, 1202
Schmidt G. D., Miller J. S., 1980, ApJ, 240, 759
Schmitt H. R., Kinney A. L., 1996, ApJ, 463, 498
Schurch N. J., Warwick R. S., 2002, MNRAS, 334, 811
Schurch N. J., Warwick R. S., Griffiths R. E., Kahn S. M., 2004, MNRAS, 350, 1
Seyfert C. K., 1943, ApJ, 97, 28

Shapovalova A. I. et al., 2008, A&A, 486, 99
Staguhn J. et al., 2018, in Lystrup M., MacEwen H. A., Fazio G. G., eds, Proc. SPIE Conf. Ser. Vol. 10698, Space Telescopes and Instrumentation 2018: Optical, Infrared, and Millimeter Wave. SPIE, Bellingham, p. 106981A
Thompson I., Landstreet J. D., Angel J. R. P., Stockman H. S., Woolf N. J., Martin P. G., Maza J., Beaver E. A., 1979, ApJ, 229, 909
Ulrich M.-H., Boksenberg A., Bromage G. E., Clavel J., Elvius A., Penston M. V., Perola G. C., Snijders M. A. J., 1991, ApJ, 382, 483
Warwick R. S., Done C., Smith D. A., 1995, MNRAS, 275, 1003
Weisskopf M. C. et al., 2016, in den Herder J.-W. A., Takahashi T., Bautz M., eds, Space Telescopes and Instrumentation 2016: Ultraviolet to Gamma Ray. SPIE, San Diego, p. 990517
Young S., Hough J. H., Axon D. J., Bailey J. A., Ward M. J., 1995, MNRAS, 272, 513
Young S., Hough J. H., Axon D. J., Fabian A. C., Ward M. J., 1998, MNRAS, 294, 478
Zdziarski A. A., Leighly K. M., Matsuoka M., Cappi M., Mihara T., 2002, ApJ, 573, 505

This paper has been typeset from a TEX/LATEX file prepared by the author.